nature communications

Article

https://doi.org/10.1038/s41467-025-58001-3

Internal lattice oxygen sites invert product selectivity in electrocatalytic alkyne hydrogenation over copper catalysts

Received: 18 August 2024

Accepted: 10 March 2025

Published online: 24 April 2025

Check for updates

Mengyu Li[1,2,4], Yimin Jiang[1,4], Wei Chen[1,2] ✉, Yucheng Huang[3], Yingrui Lu[3], Leitao Xu[1], Shengkai Li[1], Yandong Wu[1], Zhongcheng Xia[1], Ruiqi Wang[1], Shuangyin Wang[1] & Yuqin Zou[1,2] ✉

Copper-based catalysts exhibit excellent performance of electrocatalytic alkynes hydrogenation, especially for the selective alkynes hydrogenation toward alkenes. However, the selective electrocatalytic alkynes hydrogenation toward alkanes is hard to achieve over copper-based catalysts because electron-rich Cu^0 sites are unable to adsorb and activate nucleophilic alkenes. Herein, we report a metallic copper catalyst containing internal lattice oxygen atoms for steering the selectivity of alkynes hydrogenation toward alkanes. Internal lattice oxygen atoms protect $Cu^{\delta+}$ sites from being reduced during electrocatalytic alkynes hydrogenation so that alkenes intermediates can continually be adsorbed and converted to alkanes on stable $Cu^{\delta+}$ sites. Due to the synergy between Cu^0 and $Cu^{\delta+}$ sites, metallic copper electrocatalyst containing internal lattice oxygen atoms shows an excellent selectivity for selective alkynes hydrogenation toward alkanes (2-methyl-3-butan-2-ol selectivity of 94.9%). This work opens a avenue for steering the selective alkynes hydrogenation, and more importantly, it fills in a gap on the selective electrocatalytic alkynes hydrogenation toward alkanes over copper-based catalysts.

Selective hydrogenation of alkynes plays an important role in the industrial production of pharmaceuticals, petrochemicals, fragrances, agrochemicals, etc[1–6]. Growing levels of environmental pollution and energy crisis are prompting chemists to develop green and economical synthesis methods. Electrocatalytic technology is an appealing approach to realize the selective hydrogenation of alkynes at ambient temperature and pressure[7–9]. Because clean electrons and water are used as the reducing agents and hydrogen source, respectively, electrocatalytic alkynes hydrogenation (EAH) exhibits obvious advantages over the traditional routes, such as environmental friendliness, operational simplicity, safety, sustainability, and low energy consumption[5,6,10–14]. EAH involves the conversion of various organic functional groups, e.g., carbon-carbon triple bond (C≡C) and carbon-carbon double bond (C=C), and there are two main types of hydrogenation products for EAH, i.e., alkenes and alkanes. Although selective EAH toward alkenes has been widely reported, there is scarce study on the selective EAH toward alkanes. Selective hydrogenation of alkynes to alkanes not only achieves the synthesis of value-added chemicals, such as butane-1,4-diol (BAD), but also realizes the directional conversion of carbon-carbon triple bonds to carbon-carbon single bonds. The key to develop selective electrocatalytic hydrogenation is to understand and apply the structure-activity relationship between electrocatalysts and reaction pathways, which is just a difficult point in the field of EAH.

[1]State Key Laboratory of Chemo and Biosensing, College of Chemistry and Chemical Engineering, Advanced Catalytic Engineering Research Center of the Ministry of Education, Hunan University, Changsha, Hunan, PR China. [2]Greater Bay Area Institute for Innovation, Hunan University, Guangzhou, PR China. [3]National Synchrotron Radiation Research Center, Hsinchu, Taiwan, ROC. [4]These authors contributed equally: Mengyu Li, Yimin Jiang. ✉e-mail: weichen1@hnu.edu.cn; yuqin_zou@hnu.edu.cn

Due to the advantages of excellent hydrogenation performance and low cost, Cu-based catalysts have been widely used in the field of EAH[10,15]. Electronic structure of active site decides adsorption behavior, catalytic activity, and reaction pathway, etc. According to the charge distribution, Cu sites of Cu-based catalysts can be divided into two categories, including (1) nucleophilic Cu^0 sites and (2) electrophilic $Cu^{\delta+}$ sites. As for organic molecules, C≡C bond is electrophilic, while C=C bond is nucleophilic[2,16]. Hence, nucleophilic Cu^0 sites have a specific adsorption of alkynes containing C≡C bonds due to the electrostatic force[7,17,18]. On the other hand, Cu^0 sites repel each other with alkenes containing C=C bonds because of electrostatic repulsion[7,16]. As above two reasons, electron-rich metallic Cu catalysts exhibit excellent activity and selectivity for the selective EAH toward alkenes[7,16,18–21]. However, it is difficult to catalyze the electrocatalytic hydrogenation of alkynes to alkanes on electron-rich metallic Cu catalysts[7,22].

Electrophilic $Cu^{\delta+}$ sites possess a specific adsorption of alkenes containing nucleophilic C=C bonds[1], and electrophilic C≡C bonds in alkynes cannot be adsorbed by $Cu^{\delta+}$ sites. Theoretically, $Cu^{\delta+}$ sites can only catalyze electrocatalytic hydrogenation of alkenes, instead of alkynes. Electron-deficient $Cu^{\delta+}$ species have high theoretical reduction potentials (E^{θ} (Cu^{+}/Cu^{0}) = 0.521 V; E^{θ} (Cu^{2+}/Cu^{0}) = 0.342 V)[23]; however, the reaction potential of EAH is generally below −0.1 V versus reversible hydrogen electrode (V_{RHE}). Hence, the electroreduction of $Cu^{\delta+}$ sites usually take precedence over EAH, thus leading to the fast conversion of $Cu^{\delta+}$ sites to Cu^0 sites during EAHs on electron-deficient Cu-based pre-catalysts[24–26]. That is, generally, as to EAHs on electron-deficient Cu-based pre-catalysts, the real active sites are still Cu^0 sites, rather than initial $Cu^{\delta+}$ sites. It is also the reason why the main product is alkenes, rather than alkanes, for EAH on electron-deficient Cu-based pre-catalysts[8]. As a result, the selective EAH toward alkanes is one of the most challenging tasks in the field of EAH on Cu-based catalysts, and the key is the synergistic effect of electrophilic $Cu^{\delta+}$ and nucleophilic Cu^0 sites. The difficulty of the selective EAH toward alkanes lies in how to protect $Cu^{\delta+}$ sites from being reduced to guarantee the conversion of alkenes to alkanes on $Cu^{\delta+}$ sites during EAH.

In this work, we design a unique Cu catalyst containing internal lattice oxygen atoms (O-Cu NPs) via the solvothermal reduction approach. O-Cu NPs catalyst favors the selective EAH toward alkanes, while other Cu-based nano-materials are ususally active catalysts for the selective EAH toward alkenes. Multiple characterizations show that copper oxides (e.g., Cu_2O and CuO) materials can be converted to metallic Cu materials during pre-reduction. First-principles calculations prove that nucleophilic Cu^0 sites can only adsorb and activate electrophilic alkynes, instead of nucleophilic alkenes. Hence, both metallic Cu and copper oxides are good catalysts for the selective EAH toward alkenes. As to O-Cu NPs, the metal shell protects internal lattice oxygen atoms from being reduced, thus guaranteeing the continuous operation of stable $Cu^{\delta+}$ sites bonded with internal lattice oxygen atoms during EAH. According to quartz crystal microbalance (QCM) and confirmatory experiments results, stable $Cu^{\delta+}$ sites in O-Cu NPs can not only adsorb alkenes, but also catalyze the electroredution of alkenes to alkanes. Internal lattice oxygen sites invert product selectivity in electrocatalytic hydrogenation of alkynes on O-Cu NPs, thus showing an excellent selectivity for the selective EAH toward alkanes (e.g., the 2-methyl-3-butan-2-ol (MBA) selectivity of 94.9% at −0.3 V_{RHE}). Our finding opens an avenue to steer the selective EAH by regulating the interaction between Cu^0 and $Cu^{\delta+}$ sites, and more importantly, it fills in a gap on the selective EAH toward alkanes over copper-based catalysts.

Results

Selective EAH toward alkenes on Cu-based catalysts

Nucleophilic Cu^0 sites have a specific adsorption of alkynes containing C≡C bonds, and there is electrostatic repulsion between nucleophilic Cu^0 sites and alkenes containing C=C bonds. Hence, metallic Cu-based materials containing Cu^0 sites are the ideal catalysts for the selective EAH toward alkenes. As to EAHs on metallic Cu-based catalysts, electrophilic alkynes are adsorbed and electrochemically hydrogenated to generate alkenes, and then nucleophilic alkenes are rapidly desorbed from nucleophilic Cu^0 sites due to the electrostatic repulsion (Fig. 1a)[7,16]. In contrast, electrophilic $Cu^{\delta+}$ sites have a specific adsorption of nucleophilic alkenes, instead of electrophilic alkynes, so that electron-deficient Cu-based materials should be in favor of the electroreduction of alkenes to alkanes in theory (Fig. 1a)[1].

Cu, Cu_2O, and CuO nanoparticles (NPs) were synthesized as model catalysts for selective electrocatalytic hydrogenation of alkynes (Fig. 1b and Supplementary Figs. 1–3). Due to the advantages of high water-solubility and low volatility, 2-methyl-3-butyne-2-ol (MBY) was selected as the model substrate for EAH. SEM images show that Cu NPs, Cu_2O NPs and CuO NPs basically maintained the initial morphology of nanoparticles after pre-reduction (Supplementary Fig. 4). According to X-ray diffraction (XRD) patterns and X-ray photoelectron spectra (XPS), both Cu_2O NPs and CuO NPs were electrochemically reduced to metallic Cu NPs containing Cu^0 sites after pre-reduction in EAH system (Fig. 1c, d and Supplementary Figs. 5 and 6). Consequently, the active sites are metallic Cu^0 sites for EAHs on Cu, Cu_2O, and CuO NPs. As a result, Cu, Cu_2O, and CuO NPs are good catalysts for selective EAH toward alkenes. The selectivities of 2-methyl-3-buten-2-ol (MBE) are greater than 70%, while the selectivities of MBA are less than 30% at different potentials for EAHs on Cu NPs, Cu_2O NPs, and CuO NPs (Fig. 1e and Supplementary Figs. 7 and 8). Different from Cu_2O and CuO NPs, initial Cu^0 sites on Cu NPs are the active sites for EAH so that Cu NPs shows the highest MBE selectivity (e.g., 91% at −0.5 V_{RHE}) for the selective EAH toward alkenes.

Due to the differences in adsorption characteristics of alkynes and alkenes on $Cu^{\delta+}$ sites, electrophilic $Cu^{\delta+}$ species can only catalyze the electrocatalytic hydrogenation of nucleophilic alkenes to alkanes[1], instead of the electrocatalytic hydrogenation of electrophilic alkynes, in theory. In fact, during EAHs, electron-deficient $Cu^{\delta+}$ species (e.g., Cu_2O and CuO NPs) are preferentially converted to electron-rich Cu^0 species in the pre-reduction process[26,27], and then Cu^0 sites catalyze the selective EAH toward alkenes (Fig. 1f). Due to the electrostatic repulsion, electron-rich Cu^0 sites cannot adsorb nucleophilic alkenes so that it is infeasible for the electroreduction of alkenes to alkanes on Cu^0 sites. The result is that almost all of the reported Cu-based materials can only catalyze the selective EAH toward alkenes. It is urgent for researchers to develop a kind of Cu-based catalysts for the selective EAH toward alkanes.

Fabricating internal lattice oxygen atoms in O-Cu NPs

The selective EAH toward alkanes is very difficult on Cu-based catalysts, and the key problem of design is how to protect $Cu^{\delta+}$ sites from being reduced to guarantee the adsorption and electroreduction of alkenes[28–31]. Both hydrogen-thermal reduction method and electroreduction treatment have a strong reduction ability; hence, via heating in Ar/H_2 atmosphere or electrochemical reduction, electron-deficient Cu_xO_y materials (e.g., Cu_2O and CuO NPs) can be completely transformed to metallic Cu catalyst, which is unable to drive the selective EAH toward alkanes (Fig. 2a). In this work, organic solvothermal reduction method with weaker reduction ability was carried out to synthesize Cu-based catalysts containing both Cu^0 and $Cu^{\delta+}$ sites (Fig. 2b). During the process of hydrothermal reaction, Cu^{2+} ions were converted to electron-deficient Cu_xO_y solid material, and then Cu_xO_y species was slowly reduced in N, N-dimethylformamide (DMF), thus obtaining metallic Cu catalyst containing minor internal lattice oxygen atoms (O-Cu NPs).

Due to steric hindrance effect and weak reducibility of DMF, some internal lattice oxygen atoms in O-Cu NPs cannot be reduced so that there are some stable $Cu^{\delta+}$ sites on the surface of O-Cu NPs (Fig. 2b). The concentration of internal lattice oxygen atoms in O-Cu NPs can be

https://doi.org/10.1038/s41467-025-58001-3

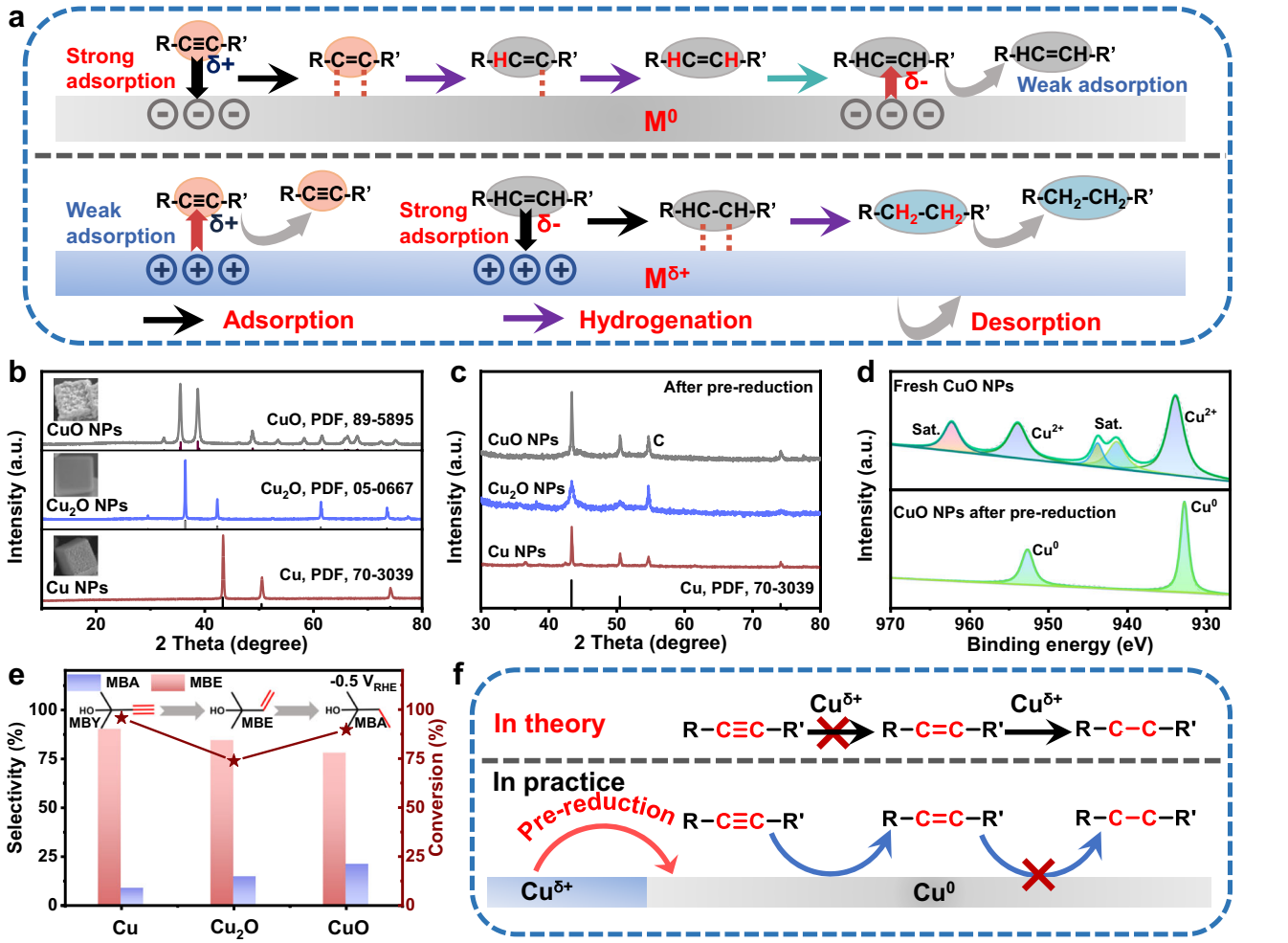

Fig. 1 | Reaction mechanism of selective EAH toward alkenes over Cu-based catalysts. a Reaction mechanism for EAH on electron-rich Cu^0 sites or electron-deficient $Cu^{\delta+}$ sites. XRD patterns of Cu NPs, Cu_2O NPs and CuO NPs **b** before and **c** after pre-reduction. **d** Cu 2*p* XPS spectra of fresh CuO NPs and CuO NPs after pre-reduction. **e** Electrocatalytic performance of MBY hydrogenation on Cu NPs, Cu_2O NPs and CuO NPs at −0.5 V_{RHE}. **f** Scheme illustration shows reaction mechanism of EAH on electron-deficient $Cu^{\delta+}$ sites. Source data are provided as a Source Data file.

regulated by controlling hydrothermal temperature (Supplementary Fig. 9). XRD pattern shows that the main crystalline phase of O-Cu NPs is metallic Cu (PDF#70-3039) with face-centered-cubic (fcc) structure, suggesting that there are abundant nucleophilic Cu^0 sites on the surface of O-Cu NPs (Fig. 2c). Scanning electron microscopy (SEM) and transmission electron microscopy (TEM) images show that the average diameter of irregular nanoparticle in O-Cu NPs is about 30 nm (Fig. 2d and Supplementary Figs. 10 and 11). According to high-resolution TEM (HRTEM) image, O-Cu NPs have poor crystallinity, and display abundant lattice distortion, which might be caused by internal lattice oxygen atoms (Fig. 2e).

In situ X-ray absorption spectroscopy (XAS) was performed to investigate the evolution of electronic structure and coordination environment of Cu species under EAH conditions. According to Cu K-edge X-ray absorption near-edge structure (XANES) spectra, the average oxidation state of Cu in O-Cu NPs and Cu NPs are 0.788 and 0, respectively (Supplementary Fig. 12). In situ XAS spectra show that there are few $Cu^{\delta+}$ sites for Cu NPs under EAH conditions, indicating that active sites of Cu NPs are Cu^0 sites (Fig. 2f, g and Supplementary Figs. 13–15). Fourier transform (FT) of Cu K-edge extended X-ray absorption fine structure (EXAFS) spectrum of O-Cu NPs show the Cu-O coordination (1.5 Å) the Cu-Cu coordination (2.2 Å), and the coordination numbers of Cu-O and Cu-Cu bonds are 2.2 and 4.9, respectively (Supplementary Figs. 16, 17)[28,32,33]. Cu-O bonds of O-Cu NPs originated from the contribution of internal lattice oxygen atoms and surface CuO_x species.

In situ Cu K-edge XANES spectra demonstrate that the oxidation state of Cu in O-Cu NPs decreases from 0.788 (OCP) to 0.251 (−0.4 V_{RHE}), which can be attributed to the electroreduction of CuO_x species on the surface of O-Cu NPs (Fig. 2f and Supplementary Figs. 18, 19). According to in situ FT-EXAFS spectra of O-Cu NPs, the intensity of the Cu-Cu coordination increased while the intensity of the Cu-O coordination slightly decreased when the reduction potential was carried out, which also supports the electroreduction of surface CuO_x species (Fig. 2h and Supplementary Figs. 20, 21). However, the Cu-O coordination can be observed in situ FT-EXAFS spectra of O-Cu NPs under EAH conditions (−0.3 and −0.4 V_{RHE}), and those stable Cu-O bonds are attributed to $Cu^{\delta+}$ site bonded with internal lattice oxygen atoms. EXAFS fitting result shows the coordination numbers of Cu-O and Cu-Cu bonds in O-Cu NPs under EAH conditions (Supplementary Fig. 22 and Supplementary Table 1). Although CuO_x species on the surface of O-Cu NPs will be reduced to Cu^0 species at reduction potentials during EAH, and $Cu^{\delta+}$ sites bonded with internal lattice oxygen atoms are rather difficult to be reduced electrochemically (Supplementary Fig. 23). Stable $Cu^{\delta+}$ sites bonded with internal lattice oxygen atoms can be act as active sites for the reaction of EAH toward alkanes on O-Cu NPs owing to the excellent stability at reduction potentials.

https://doi.org/10.1038/s41467-025-58001-3

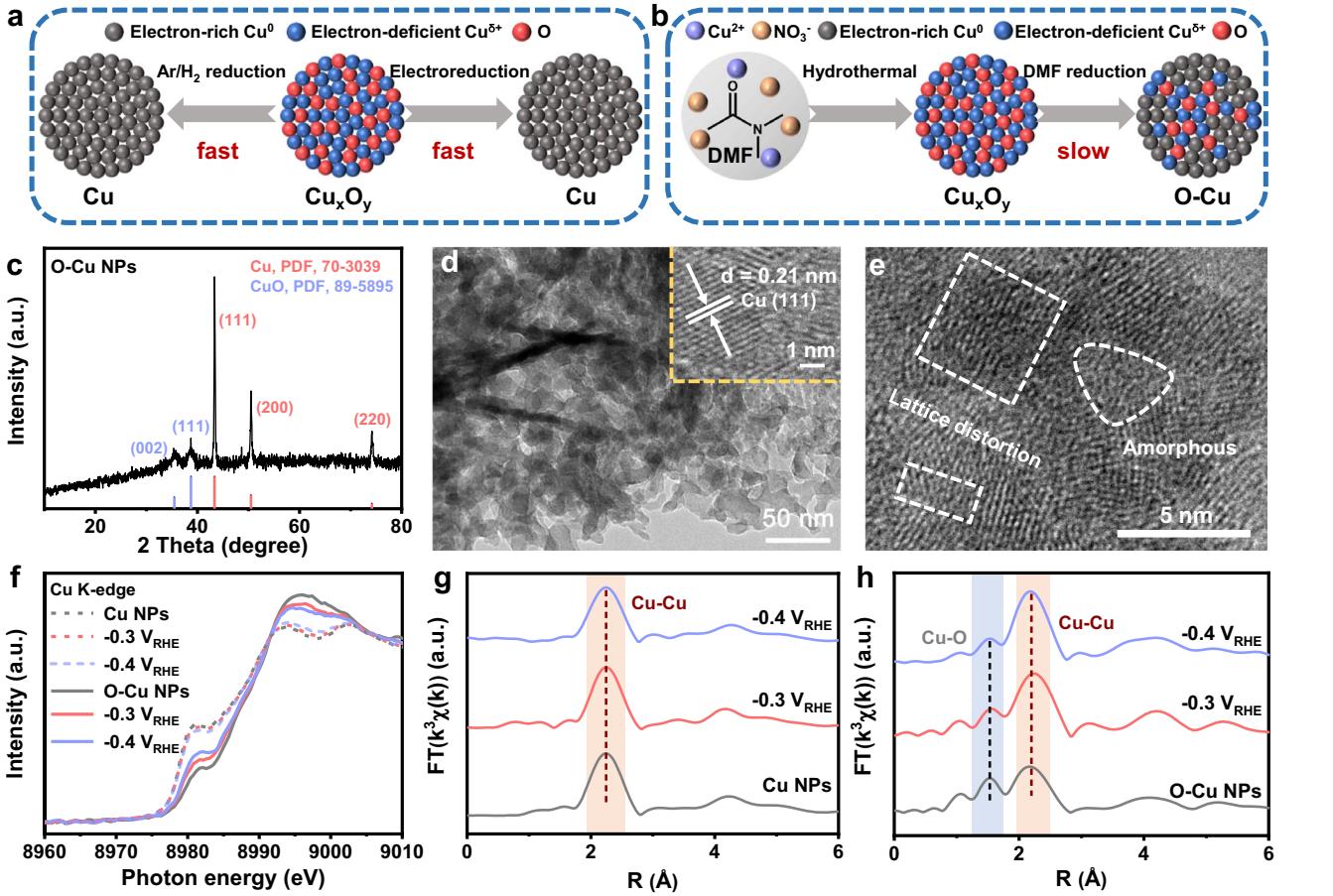

Fig. 2 | Morphological and structural characterizations of O-Cu NPs. Scheme illustration shows the reduction treatment of Cu-based oxides under **a** strong reduction conditions and **b** weak reduction condition. **c** XRD pattern, **d** TEM image, and **e** HRTEM image of O-Cu NPs. **f** Normalized in situ Cu K-edge XANES spectra of O-Cu NPs and Cu NPs in 1 M KOH at different potentials. FT-EXAFS spectra of **g** Cu NPs and **h** O-Cu NPs in 1 M KOH with MBY at different potentials. Source data are provided as a Source Data file.

Selective EAH toward alkanes for O-Cu NPs

O-Cu NPs catalyst exhibits higher apparent and intrinsic activities of EAH than Cu NPs catalyst so that the electrolysis efficiency of EAH on O-Cu NPs is higher than that on Cu NPs (Fig. 3a and Supplementary Figs. 24–28). To reveal the reaction pathways of EAHs on Cu NPs and O-Cu NPs, the concentration changes of MBY, MBE, and MBA were measured during EAH (constant-current electrolysis at -20 mA cm^{-2}). During EAH on Cu NPs, MBY was quickly converted to MBE while MBE was hard to be further hydrogenated to MBA, suggesting Cu NPs catalyst is in favor of the selective EAH toward alkenes (Fig. 3b). The MBE selectivity for EAH on Cu NPs is decreased slightly as the potentials become more negative, because higher negative potentials can cause the over-hydrogenation of MBE to MBA (Fig. 3c). For example, as to EAH over Cu NPs at the potential of −0.5 V_{RHE}, MBY conversion and MBE selectivity are 95.7% and 90.6%, respectively. In addition, yield and Faradic efficiency (FE) for selective EAH toward alkenes over Cu NPs at −0.5 V_{RHE} are 86.8% and 10.8%, respectively (Supplementary Figs. 29a and 30a).

On the contrary, the selective EAH toward alkanes is more favorable than that toward alkenes on O-Cu NPs catalyst, which is different from the vast majority of Cu-based materials. For EAH over O-Cu NPs at the potential of −0.3 V_{RHE}, MBY conversion and MBA selectivity are 98.3% and 94.9%, respectively. In addition, yield and FE for selective EAH toward alkanes over O-Cu NPs at −0.3 V_{RHE} are 93.2% and 23.2%, respectively (Supplementary Figs. 29b and 30b). During EAH on O-Cu NPs, MBA was generated quickly while the concentration of MBE is lower, indicating that the reaction rate for electrocatalytic hydrogenation of MBE to MBA far outweighed that for the hydrogenation of MBY to MBE (Fig. 3d). Stable $Cu^{\delta+}$ sites are necessary for the adsorption and electroreduction of alkenes. High MBA selectivity of EAH on O-Cu NPs indirectly proves the high stability of $Cu^{\delta+}$ sites bonded with internal lattice oxygen atoms[34], and stable $Cu^{\delta+}$ sites efficiently catalyze the electroreduction of MBE to MBA. MBY conversion and the MBA selectivity for EAH on O-Cu NPs is decreased slightly as the potentials become more negative, because adsorbed hydrogen species (H*) prefers competitive hydrogen evolution reaction (HER) to EAH as the applied potentials become more negative[35,36]. Competitive HER is more favorable at more negative potentials, alkynes hydrogenation is weakened (Fig. 3e, Supplementary Fig. 31 and Table 2).

Furthermore, O-Cu NPs catalyst shows excellent stability in terms of electrochemical MBY hydrogenation activity and MBA selectivity during continuous five electrolysis cycles at the potential of −0.3 V_{RHE} (Fig. 3f). According to XRD pattern, SEM and TEM images, O-Cu NPs basically maintained its initial crystal structure and morphology without obvious agglomeration after long-term stability measurement (Supplementary Figs. 32–34). HRTEM image of O-Cu NPs after electrolysis shows internal lattice oxygen atoms induced localized disordered lattice structure, indicating that internal lattice oxygen atoms in O-Cu NPs are relatively stable during long-term stability measurement (Supplementary Fig. 34d). Internal lattice oxygen atoms own the characteristic of high stability so that stable $Cu^{\delta+}$ sites bonded with internal lattice oxygen atoms can drive the electroreduction of alkenes to alkanes. The synergistic effect of electron-rich Cu^0 sites and

https://doi.org/10.1038/s41467-025-58001-3

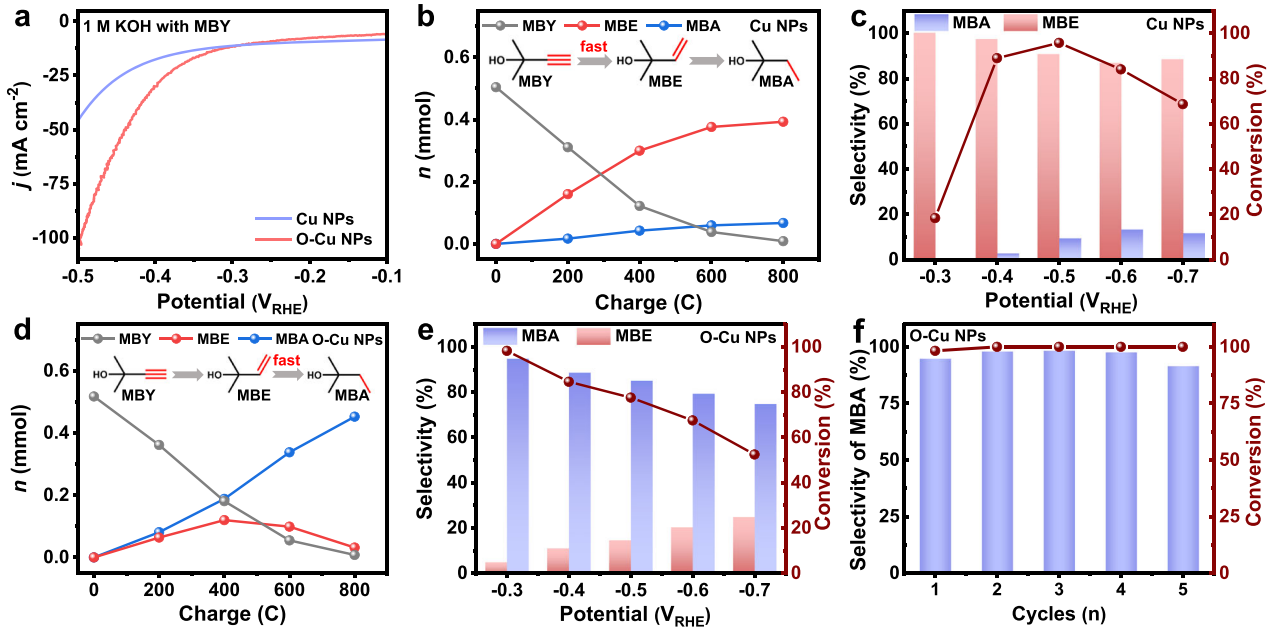

Fig. 3 | Electrocatalytic performance for EAH on Cu-based catalysts. **a** Polarization curves of Cu NPs and O-Cu NPs in 1 M KOH electrolyte with the addition of MBY. **b** Charge-dependent moles of MBY, MBE, and MBA during electrocatalytic MBY hydrogenation at −20 mA cm^{-2} using Cu NPs. **c** MBY conversions, MBE and MBA selectivities on Cu NPs at various potentials. **d** Charge-dependent moles of MBY, MBE, and MBA during electrocatalytic MBY hydrogenation at −20 mA cm^{-2} using O-Cu NPs. **e** MBY conversions, MBE and MBA selectivities on O-Cu NPs at various potentials. **f** Cycling stability of electrocatalytic MBY hydrogenation on O-Cu NPs at the potential of −0.3 V_{RHE}. Source data are provided as a Source Data file.

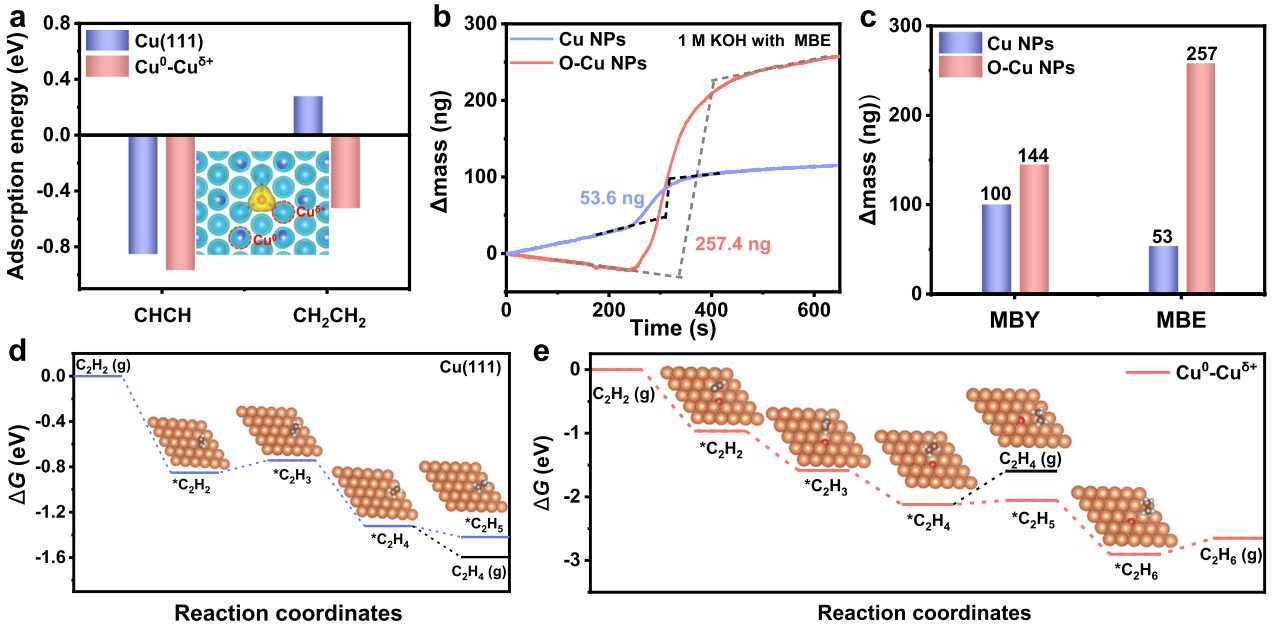

Fig. 4 | Theoretical and experimental insight into the reaction mechanism. **a** The adsorption energy of acetylene and ethylene on Cu(111) and Cu^0-$Cu^{\delta+}$ sites. **b** QCM mass response over O-Cu NPs and Cu NPs catalysts in 1 M KOH electrolyte before and after the addition of MBE. **c** QCM mass response over O-Cu NPs and Cu NPs catalysts in 1 M KOH electrolyte after the addition of MBY or MBE. **d** The free-energy diagram for electrocatalytic hydrogenation of acetylene to ethylene on Cu^0 site in Cu(111). **e** The free-energy diagram for electrocatalytic hydrogenation of acetylene to ethane on Cu^0-$Cu^{\delta+}$ sites in O-Cu(111). Source data are provided as a Source Data file.

electron-deficient $Cu^{\delta+}$ sites is the key point to achieve selective EAH toward alkanes on O-Cu NPs.

Reaction mechanism of EAH on O-Cu NPs

There are two types of Cu sites on O-Cu NPs, i.e., (1) Cu^0 sites far from the internal lattice oxygen atom (Cu^0-O-far) and (2) $Cu^{\delta+}$ sites bonded with the internal lattice oxygen atom ($Cu^{\delta+}$-O-near). According to deformation charge density diagrams, internal lattice oxygen atoms induce the electron transfer from $Cu^{\delta+}$-O-near sites to oxygen atoms in O-Cu(111), while there is no significant charge accumulation for both Cu^0-O-far sites in O-Cu(111) and Cu^0 sites in Cu(111) (Fig. 4a and Supplementary Fig. 35). Consequently, as to O-Cu NPs, the diatomic site pair of Cu^0-$Cu^{\delta+}$ sites possess both electrophilicity and nucleophilicity. Density functional theory (DFT) calculation is carried out to

https://doi.org/10.1038/s41467-025-58001-3

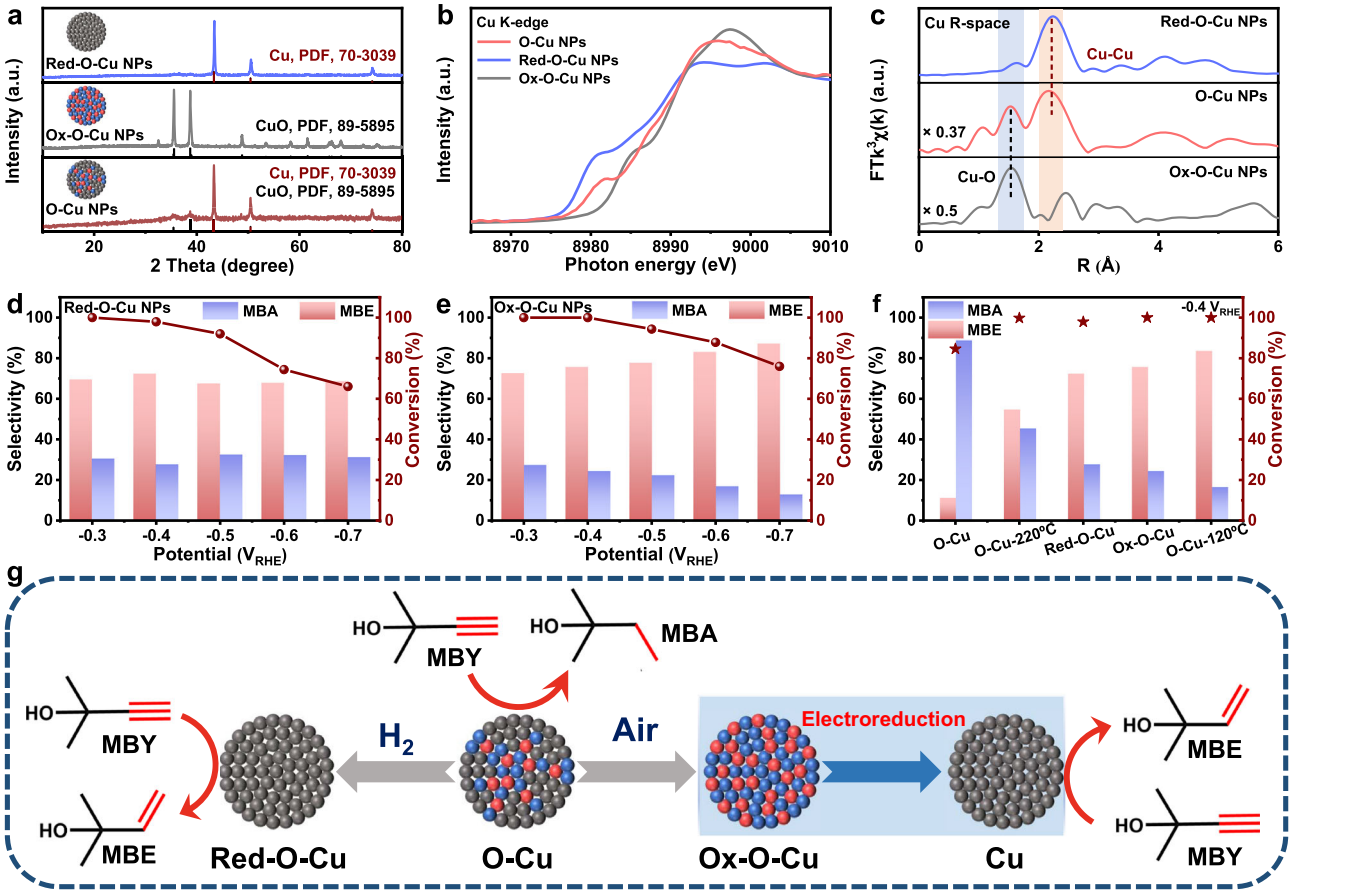

Fig. 5 | Catalytic role of internal lattice oxygen atoms for selective EAH toward alkanes. a XRD patterns, **b** Cu K-edge XANES spectra, and **c** FT-EXAFS spectra of Red-O-Cu NPs, O-Cu NPs, and Ox-O-Cu NPs. MBY conversions, MBE and MBA selectivities on **d** Red-O-Cu NPs and **e** Ox-O-Cu NPs at various potentials. **f** MBY conversions, MBE and MBA selectivities on O-Cu NPs, O-Cu NPs-220 °C, Red-O-Cu NPs, Ox-O-Cu NPs, and O-Cu NPs-120 °C at −0.4 V_{RHE}. **g** Scheme illustration of the conversion process of O-Cu NPs, Red-O-Cu NPs, and Ox-O-Cu NPs and the dominant product of electrocatalytic MBY hydrogenation. Source data are provided as a Source Data file.

understand the adsorption strength of alkynes and alkenes. As depicted in Fig. 4a, Cu^0-$Cu^{\delta+}$ sites in O-Cu(111) exhibit specific adsorption of both electrophilic alkynes (ΔG: −0.966 eV) and nucleophilic alkenes (ΔG: −0.524 eV), while Cu^0 sites in Cu(111) can only absorb alkynes containing C≡C bonds (ΔG: −0.851 eV), instead of alkenes containing C=C bonds (ΔG: 0.274 eV).

QCM measurement is performed to further identify the adsorption strength of alkynes and alkenes on Cu NPs and O-Cu NPs. Cu NPs electrode containing Cu^0 sites has a strong adsorption of MBY, rather than MBE, while O-Cu NPs electrode containing Cu^0-$Cu^{\delta+}$ sites exhibits excellent adsorption ability for both MBY and MBE, which is consistent with DFT calculation results (Fig. 4b, c and Supplementary Fig. 36). As a result, Cu NPs can only catalyze the electroreduction of alkynes, instead of alkenes, and meanwhile, both alkynes and alkenes can be electrochemically reduced on O-Cu NPs (Supplementary Fig. 37). These results sufficiently attest that the adsorption strength of alkynes and alkenes on catalysts is a key factor in determining reaction pathways of EAH. According to the free-energy diagrams of C_2H_2 hydrogenation on Cu(111), the energy barrier for $*C_2H_4$ desorption (ΔG: −0.274 eV) is much lower than that for $*C_2H_4$ hydrogenation to $*C_2H_5$ (ΔG: −0.0967 eV), indicating that Cu NPs catalyst is in favor of the selective EAH toward alkenes (Fig. 4d and Supplementary Figs. 38 and 39)[15]. On the contrary, the energy barrier for alkenes desorption ($*C_2H_4 \rightarrow C_2H_4$ (g), ΔG: 0.524 eV) on O-Cu(111) is much higher than that for alkenes activation ($*C_2H_4 \rightarrow C_2H_5$, ΔG: 0.064 eV), indicating that O-Cu NPs catalyst is in favor of the selective EAH toward corresponding alkanes (Fig. 4e and Supplementary Figs. 38 and 39), consistenting with electrochemical experiments results in Fig. 3e.

Clarifying the importance of internal lattice oxygen atoms

To verify the importance of internal lattice oxygen atoms for the selective EAH toward alkanes, we regulated the concentration of internal lattice oxygen atoms in O-Cu NPs (Supplementary Fig. 40). O-Cu NPs sample was heated in Ar/H_2 atmosphere to synthesize Red-O-Cu NPs catalyst with the crystalline phase of metallic Cu (Fig. 5a and Supplementary Figs. 41–46). XAS results further prove that thermal reduction treatment has greatly reduced the number of internal lattice oxygen atoms in Red-O-Cu NPs (Fig. 5b, c and Supplementary Figs. 44–46). Compared to O-Cu NPs, a higher coordination number of Cu-Cu bond at 2.2 Å was observed on Red-O-Cu NPs (Supplementary Fig. 47 and Supplementary Table 1). Via thermal treatment in air atmosphere, O-Cu NPs sample was oxidized to synthesize Ox-O-Cu NPs sample with the crystalline phase of CuO, which possesses abundant lattice oxygen atoms (Fig. 5a–c and Supplementary Figs. 41–46). In contrast to O-Cu NPs, Ox-O-Cu NPs exhibits a higher coordination number of Cu-O bond at about 1.5 Å (Supplementary Fig. 47 and Supplementary Table 1).

As to EAH on Red-O-Cu NPs with few internal lattice oxygen atoms, the dominant product of MBY hydrogenation is MBE, instead of MBA (Fig. 5d and Supplementary Fig. 48a). The reaction pathway of EAH on Red-O-Cu NPs is quite different from that on O-Cu NPs (Supplementary Fig. 49a), proving that internal lattice oxygen atoms play a crucial role in the selective EAH toward alkanes, especailly for the electroreduction of alkenes to alkanes. And the maximum yield of selective EAH toward alkenes on Red-O-Cu NPs is 70.8% at −0.4 V_{RHE} (Supplementary Fig. 50a). Similarly, the concentration of internal lattice oxygen atoms in O-Cu NPs can be reduced by increasing

https://doi.org/10.1038/s41467-025-58001-3

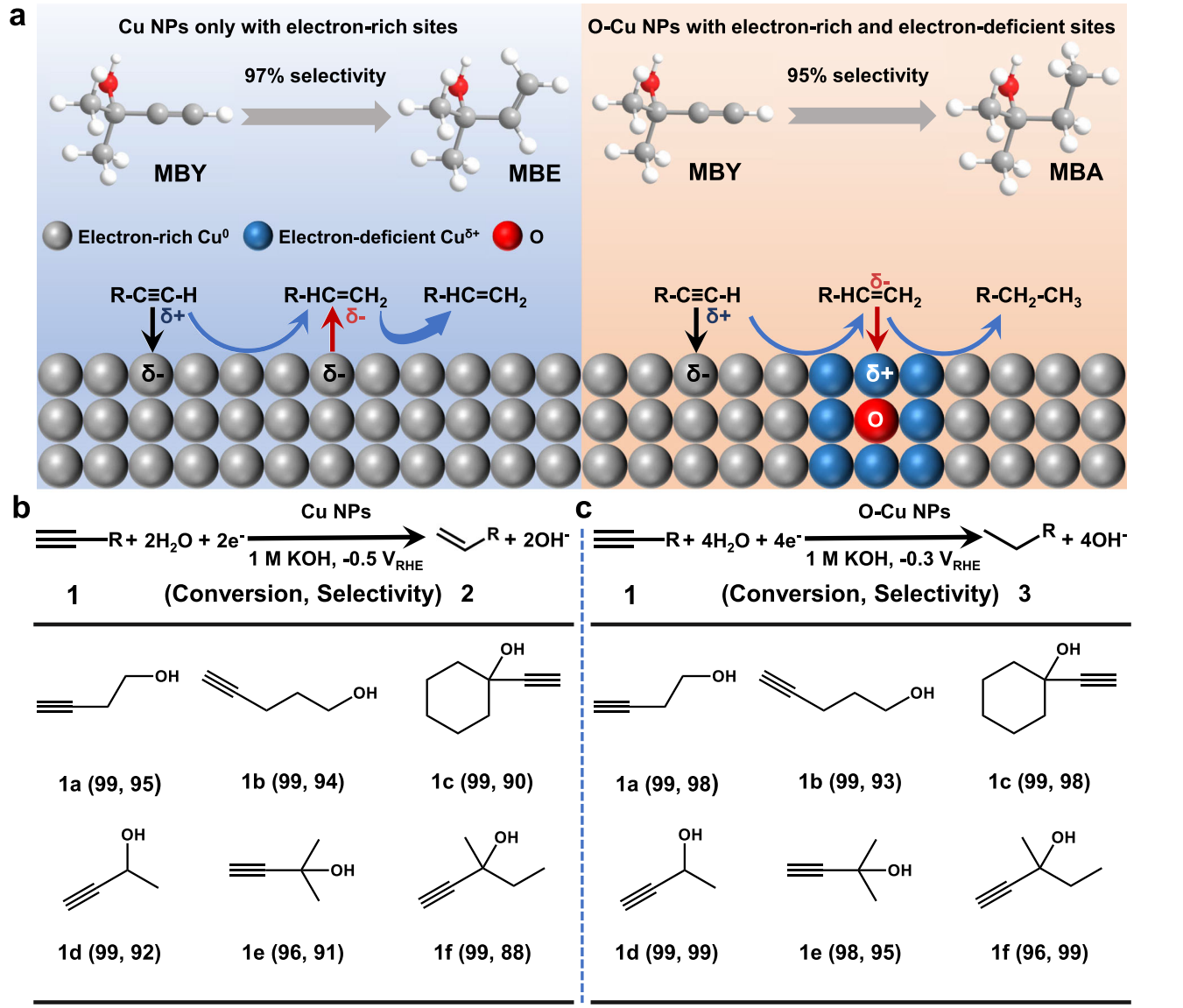

Fig. 6 | Substrate scope for selective EAH. a Scheme illustration of electrocatalytic alkynes hydrogenation on Cu NPs and O-Cu NPs. **b** Substrate scope for EAH toward alkenes on Cu NPs catalyst. **c** Substrate scope for EAH toward alkanes on O-Cu NPs catalyst.

hydrothermal temperature, thus leading to a lower alkane selectivity for EAH on O-Cu NPs-220 °C (Supplementary Figs. 9 and 51-55).

On the other hand, during EAH, Ox-O-Cu NPs with excessive lattice oxygen atoms undergoes a phase transformation process from CuO to metallic Cu containing nucleophilic Cu^0 sites, which is conducive to the desorption of nucleophilic alkenes and the selective EAH toward alkenes (Supplementary Fig. 56)[7,16]. Hence, as to MBY hydrogenation on Ox-O-Cu NPs, the dominant product is MBE as well (Fig. 5e and Supplementary Figs. 48b, 49b, and 50b). Similarly, the concentration of lattice oxygen atoms in O-Cu NPs can be increased by decreasing hydrothermal temperature, thus also leading to a higher selectivity for the EAH toward alkenes on O-Cu NPs-120 °C (Supplementary Figs. 51–55). These results prove that excessive lattice oxygen atoms can reduce the stability of $Cu^{\delta+}$ sites[18,26]. As to O-Cu NPs, the metal shell protects internal lattice oxygen atoms to guarantee the stability of $Cu^{\delta+}$ sites bonded with internal lattice oxygen. Consequently, only O-Cu NPs catalyst containing the appropriate amount of internal lattice oxygen atoms is an effective Cu-based catalyst for selective EAH toward alkanes (Fig. 5f, g).

The reacation pathway of EAH can be regulated by synergistic effect of nucleophilic Cu^0 sites and electrophilic $Cu^{\delta+}$ sites in different Cu-based catalysts. Cu NPs catlyst only containing electron-rich Cu^0 sites is an effective Cu-based catalyst for selective EAH toward alkenes because C=C bond cannot be adsorbed and converted in Cu^0 sites (Fig. 6a). The key to realize semi-hydrogenation of alkynes is based on enriching the electron density of active sites to increase the binding affinity of alkynes. Due to the synergy of stable $Cu^{\delta+}$ and Cu^0 sites, O-Cu NPs can continuously drive electroreduction of alkynes to alkenes and eventually to alkanes (Fig. 6a). To estimate the universality for selective EAH on Cu NPs and O-Cu NPs, a series of water-soluble terminal alkynols are used as the substrates. Alkenes selectivity on Cu NPs and alkanes selectivity on O-Cu NPs are always over 85% when the alkynes conversion exceeds 95% (Fig. 6b, c), exhibiting broad substrates applicability.

Discussion

In conclusion, we developed the O-Cu NPs catalyst containing internal lattice oxygen atoms for selective EAH to alkanes. As to O-Cu NPs, the metal shell protects internal lattice oxygen atoms from being reduced during the process of organic solvothermal reduction method, thus leading to stable $Cu^{\delta+}$ sites bonded with internal lattice oxygen atoms in O-Cu NPs. Both Cu NPs and CuO_x catalysts after pre-reduction with

the active phase of metallic copper can only catalyze the selective EAH to alkenes, instead of to alkanes, because electron-rich Cu^0 sites cannot adsorb and activate alkenes. Internal lattice oxygen atoms invert product selectivity in the EAH on copper catalysts. Owing to the synergy of Cu^0 and $Cu^{\delta+}$ sites, both alkynes and alkenes can be adsorbed and eletrochemically reduced on O-Cu NPs so that O-Cu NPs favors the selective EAH to alkanes. Besides, selective EAH to alkanes on O-Cu NPs shows an excellent activity, stability, and broad substrates applicability. This work illustrated the relationship between the selectivity and active site for EAH on Cu-based catalysts, and filled the gap in the study of the selective EAH toward alkanes on Cu-based catalysts.

Methods

Materials

All chemicals were used without further purification. Copper (II) chloride dihydrate ($CuCl_2{\cdot}2H_2O$, 99%), copper (II) nitrate trihydrate ($Cu(NO_3)_2{\cdot}3H_2O$, 99%), ascorbic acid (AA, 99.7%), sodium hydroxide (NaOH, 96%), potassium hydroxide (KOH, 85%), ethanol (99.7%), N, N-dimethylformamide (DMF, 99.5%) were purchased from Sinopharm Chemical Reagent Co. Ltd. Deionized (DI) water (18.25 MΩ cm) was utilized throughout the experiments.

Preparation of O-Cu NPs

In a typical synthesis of O-Cu NPs, 2 mmol $Cu(NO_3)_2{\cdot}3H_2O$ was dissolved in 50 mL DMF under vigorous stirring for 30 min. After that the mixture was transferred into a 100 mL autoclave, sealed and heated at 190 °C for 24 h. After naturally cooling to room temperature, the solid product was collected by filtering, washed with deionized water and anhydrous ethanol, and finally dried in vacuum at 60 °C, as-obtained catalyst was named as O-Cu NPs (unless otherwise stated). Other samples were prepared in a similar way with different hydrothermal temperatures and denoted as O-Cu NPs-hydrothermal temperature.

Preparation of the Red-O-Cu NPs and Ox-O-Cu NPs

O-Cu NPs catalyst was placed into a quartz tube, the furnace was heated at 300 °C for 2 h at a rate of 5 °C min^{-1} in 5% H_2-Ar atmosphere, as-obtained catalyst was recorded as Red-O-Cu NPs. O-Cu NPs catalyst was placed into a quartz tube, O-Cu NPs was oxidized by exposing in air atmosphere at 500 °C for 2 h at a rate of 5 °C min^{-1}, as-synthesized catalyst was recorded as Ox-O-Cu NPs.

Preparation of Cu_2O NPs

In a typical procedure[37], 0.341 g $CuCl_2{\cdot}2H_2O$ (2 mmol) was sufficiently mixed with 200 mL deionized water, the solution was heated at 55 °C for 30 min under vigorous stirring. After that, 20 mL of 2 M NaOH was added to the above solution with the injection rate of 120 mL h^{-1} and stirred for 30 min. Then, 20 mL of 0.6 M ascorbic acid aqueous solution with the injection rate of 120 mL h^{-1} was added under continuous stirring. Finally, the solution was aged at 55 °C for 3 h. To get Cu_2O NPs, the precipitate was collected by filtering, washed with deionized water and anhydrous ethanol, and dried in vacuum at 60 °C.

Preparation of Cu NPs and CuO NPs

To synthesize Cu NPs, Cu_2O NPs was calcined in a tube furnace in 5% H_2-Ar atmosphere, the furnace was heated at 300 °C and maintained for 2 h at a rate of 5 °C min^{-1}. To synthesize CuO NPs, Cu_2O NPs was calcined in a tube furnace in air atmosphere, the furnace was heated at 500 °C for 1 h at a rate of 5 °C min^{-1}.

Characterizations

Powder XRD was recorded on a Bruker D8-Advance X-ray diffractometer with Cu Kα radiation (1.54056 Å). XPS measurement was performed on an Escalab 250Xi X-ray photoelectron spectrometer using monochromatic Al Kα radiation. SEM image was collected in a Hitachi S4800. TEM was performed on a thermofisher F200i. QCM measurement was performed on a QSense explorer (Biolin Scientific) at room temperature using Au-coated quartz sensors. XAS of Cu K-edge and R-space was conducted at BL17C at the National Synchrotron Radiation Research Center, Taiwan.

Electrochemical measurements

Electrochemical measurements were performed on an Ivium electrochemical worksation at room temperature. EAH was conducted in an H-cell with pre-treated Nafion 117 as separator. Each chamber contained 35 mL 1 M KOH aqueous solution, and 50 μL MBY was added to the cathode chamber. Working electrode was Cu-based catalysts loaded on carbon paper (1 cm^2, HCP030N), Pt mesh was used as counter electrode and Hg/HgO acted as reference electrode. All potentials were converted to RHE according to the Nernst equation:

$$E(\mathrm{RHE}) = E(\mathrm{Hg/HgO,\ 1\,M\,KOH}) + 0.098\,\mathrm{V} + 0.059\,\mathrm{V} \times \mathrm{pH} \quad (1)$$

Typically, 4 mg catalyst was dispersed into a mixture containing 500 μL deionized water and 450 μL ethanol, and then 50 μL Nafion solution (5 wt.%) was added with ultrasonic treatment for least 15 min. After that 200 μL of homogeneous catalyst ink was drop-cast onto carbon paper with a loading of 0.8 mg cm^{-2}. Linear sweep voltammetry was carried out at the scan rate of 5 mV s^{-1} in 1 M KOH aqueous solution with or without the addition of MBY with 80% *iR*-compensation. Cyclic voltammetry was performed at the scan rate of 20 mV s^{-1}. Chronoamperometry was tested at various potentials from −0.3 to −0.7 V_{RHE} until the total amount of charge passing through the cathode was 800 C. After electrolysis, the electrolyte (1 mL) at the cathode chamber are extracted by 1 mL ethyl acetate for three times to obtain 3 mL of ethyl acetate solution containing hydrogenation products, the residual water in ethyl acetate phase is dried with anhydrous Na_2SO_4. The amount of MBE and MBA produced by electrocatalytic MBY hydrogenation were analyzed by gas chromatography (GC 2014, Shimadzu) using flame ionization detector equipped with a SH-Wax column. Then the conversion of MBY, selectivity, yield, and FE of MBE and MBA were calculated according to the standard curves. Electrochemical impedance spectroscopy was conducted at the potential of −0.3 V_{RHE} with frequencies range from 100 kHz to 0.01 Hz.

DFT calculation

All the DFT calculations[38] in this work were performed by the Vienna Ab Initio Simulation Package (VASP)[39] version 5.4. The core-electron interaction were described by the projector augmented wave (PAW) method[40]. The exchange correlation functional is described by Perdew-Burke-Ernzerhof (PBE)[41] in the generalized gradient approximation (GGA). The framework of the projector-augment wave measurement was considered with the energy cut off at 500 eV. Using the Gamma scheme with a sampling density of 0.02 for the bulk and 0.04 for all other surfaces and adsorption models, 1×10^{-5} eV $cell^{-1}$ in total energy, and 0.03 eV $Å^{-1}$ in force was adopted for the convergence criterion during structural optimization. The vacuum space along the z direction was set to 15 Å, which was sufficient to avoid interactions between the two neighboring images. The Gibbs free energy was described by $\Delta G = \Delta E - T\Delta S + \Delta ZPE$. The adsorption energies were calculated according to the equation, $E\mathrm{ads} = E(\mathrm{adsorbate/substrate}) - [E(\mathrm{substrate}) + E(\mathrm{adsorbate})]$, where E(adsorbate/substrate), E(substrate), and E(adsorbate) represent the total energy of substrate with adsorbed species, the clean substrate, and the molecule in the gas phase, respectively. Atomic charges were computed using the atom-in-molecule scheme proposed by Bader[42,43]. The deformation charge density is calculated by the difference between the total valence charge density of the structure and the superposition of the valence charge densities of neutral atoms. Deformation charge density was post-processed by VASPKIT[44] and visualized by VESTA[45], an open source software.

Data availability

The data that support the findings of this study are included in the published article and its Supplementary Information. All other data are available from the authors upon reasonable request. Source data are provided with this paper.

References

1. Xing, C. et al. Highly selective electrocatalytic olefin hydrogenation in aqueous solution. *Angew. Chem. Int. Ed.* **62**, e202310722 (2023).
2. Zhang, L., Zhou, M., Wang, A. & Zhang, T. Selective hydrogenation over supported metal catalysts: from nanoparticles to single atoms. *Chem. Rev.* **120**, 683–733 (2020).
3. Chen, X., Shi, C. & Liang, C. Highly selective catalysts for the hydrogenation of alkynols: a review. *Chin. J. Catal.* **42**, 2105–2121 (2021).
4. Mao, S. et al. Tuning the catalytic performance for the semi-hydrogenation of alkynols by selectively poisoning the active sites of Pd catalysts. *Green. Chem.* **21**, 4143–4151 (2019).
5. Ling, Y. et al. Selenium vacancy promotes transfer semihydrogenation of alkynes from water electrolysis. *ACS Catal.* **11**, 9471–9478 (2021).
6. Zhao, Y. et al. Dopant- and surfactant-tuned electrode-electrolyte interface enabling efficient alkynol semi-hydrogenation. *J. Am. Chem. Soc.* **145**, 6516–6525 (2023).
7. Bu, J. et al. Selective electrocatalytic semihydrogenation of acetylene impurities for the production of polymer-grade ethylene. *Nat. Catal.* **4**, 557–564 (2021).
8. Shi, R. et al. Room-temperature electrochemical acetylene reduction to ethylene with high conversion and selectivity. *Nat. Catal.* **4**, 565–574 (2021).
9. Han, C. et al. Electrocatalytic hydrogenation of alkenes with Pd/carbon nanotubes at an oil-water interface. *Nat. Catal.* **5**, 1110–1119 (2022).
10. Wu, Y. et al. Converting copper sulfide to copper with surface sulfur for electrocatalytic alkyne semi-hydrogenation with water. *Nat. Commun.* **12**, 3881 (2021).
11. Xu, X. et al. Regulating the interfacial water structure by tensile strain to boost electrochemical semi-hydrogenation of alkynes. *Inorg. Chem. Front.* **9**, 3444–3452 (2022).
12. Wu, Y., Liu, C., Wang, C., Lu, S. & Zhang, B. Selective transfer semihydrogenation of alkynes with H_2O (D_2O) as the H (D) source over a Pd-P cathode. *Angew. Chem. Int. Ed.* **59**, 21170–21175 (2020).
13. Guo, S. et al. Electrocatalytic hydrogenation of quinolines with water over a fluorine-modified cobalt catalyst. *Nat. Commun.* **13**, 5297 (2022).
14. Liu, H. et al. Unraveling electroreductive mechanisms of biomass-derived aldehydes via tailoring interfacial environments. *ACS Catal.* **12**, 14072–14085 (2022).
15. Jiang, X. et al. Cu single-atom catalysts for high-selectivity electrocatalytic acetylene semihydrogenation. *Angew. Chem. Int. Ed.* **62**, e202307848 (2023).
16. Zhang, L. et al. Efficient electrocatalytic acetylene semihydrogenation by electron-rich metal sites in N-heterocyclic carbene metal complexes. *Nat. Commun.* **12**, 6574 (2021).
17. Gao, Q. et al. Atomic layers of B2 CuPd on Cu nanocubes as catalysts for selective hydrogenation. *J. Am. Chem. Soc.* **145**, 19961–19968 (2023).
18. Bu, J. et al. Highly selective electrocatalytic alkynol semihydrogenation for continuous production of alkenols. *Nat. Commun.* **14**, 1533 (2023).
19. An, S. et al. Functional aqueous zinc-acetylene batteries for electricity generation and electrochemical acetylene reduction to ethylene. *Angew. Chem. Int. Ed.* **61**, e202116370 (2022).
20. Xue, W. et al. Electrosynthesis of polymer-grade ethylene via acetylene semihydrogenation over undercoordinated Cu nanodots. *Nat. Commun.* **14**, 2137 (2023).
21. Wang, S. et al. Highly efficient ethylene production via electrocatalytic hydrogenation of acetylene under mild conditions. *Nat. Commun.* **12**, 7072 (2021).
22. Bai, R. et al. Weak acetylene adsorption terminated carbon-carbon coupling kinetics on silver electrocatalysts. *CCS Chem.* **5**, 200–208 (2022).
23. Zhang, L. et al. Oxophilicity-controlled CO_2 electroreduction to C_{2+} alcohols over Lewis acid metal-doped $Cu^{\delta+}$ catalysts. *J. Am. Chem. Soc.* **145**, 21945–21954 (2023).
24. Bai, L. et al. Efficient industrial-current-density acetylene to polymer-grade ethylene via hydrogen-localization transfer over fluorine-modified copper. *Nat. Commun.* **14**, 8384 (2023).
25. Zhao, B. H. et al. Economically viable electrocatalytic ethylene production with high yield and selectivity. *Nat. Sustain.* **6**, 827–837 (2023).
26. Chen, C. et al. Boosting the productivity of electrochemical CO_2 reduction to multi-carbon products by enhancing CO_2 diffusion through a porous organic cage. *Angew. Chem. Int. Ed.* **61**, e202202607 (2022).
27. Zhang, W. et al. Rh-dispersed Cu nanowire catalyst for boosting electrocatalytic hydrogenation of 5-hydroxymethylfurfural. *Sci. Bull.* **68**, 2190–2199 (2023).
28. Zheng, J. et al. Ambient-pressure synthesis of ethylene glycol catalyzed by C_{60}-buffered Cu/SiO_2. *Science* **376**, 288–292 (2022).
29. Zhang, J. et al. Grain boundary-derived Cu^+/Cu^0 interfaces in CuO nanosheets for low overpotential carbon dioxide electroreduction to ethylene. *Adv. Sci.* **9**, 2200454 (2022).
30. Ren, Y. et al. Synergetic effect of Cu^0-Cu^+ derived from layered double hydroxides toward catalytic transfer hydrogenation reaction. *Appl. Catal. Environ.* **314**, 121515 (2022).
31. Yuan, X. et al. Controllable Cu^0-Cu^+ sites for electrocatalytic reduction of carbon dioxide. *Angew. Chem. Int. Ed.* **60**, 15344–15347 (2021).
32. Yang, R. et al. In situ halogen-ion leaching regulates multiple sites on tandem catalysts for efficient CO_2 electroreduction to C_{2+} products. *Angew. Chem. Int. Ed.* **61**, e202116706 (2022).
33. Li, Q. et al. Efficient CO_2 electroreduction to multicarbon products at $CuSiO_3$/CuO derived interfaces in ordered pores. *Adv. Mater.* **35**, 2305508 (2023).
34. Wei, C. et al. Lattice oxygen-mediated electron tuning promotes electrochemical hydrogenation of acetonitrile on copper catalysts. *Nat. Commun.* **14**, 3847 (2023).
35. Bi, X. et al. Electroreduction of CO_2 to C_2H_4 regulated by spacing effect: mechanistic insights from DFT studies. *Energy Mater. Adv.* **4**, 0037 (2023).
36. Gao, Y., Wang, E., Zheng, Y., Zhou, J. & Sun, Z. Hexagonal MBenes-supported single atom as electrocatalysts for the nitrogen reduction reaction. *Energy Mater. Adv.* **4**, 0039 (2023).
37. Zhang, D. F. et al. Delicate control of crystallographic facet-oriented Cu_2O nanocrystals and the correlated adsorption ability. *J. Mater. Chem.* **19**, 5220–5225 (2009).
38. Kohn, W. & Sham, L. J. Self-consistent equations including exchange and correlation effects. *Phys. Rev.* **140**, A1133–A1138 (1965).
39. Kresse, G. & Hafner, J. Ab initio molecular dynamics for open-shell transition metals. *Phys. Rev. B* **48**, 13115–13118 (1993).
40. Blöchl, P. E. Projector augmented-wave method. *Phys. Rev. B* **50**, 17953–17979 (1994).
41. Perdew, J. P., Burke, K. & Ernzerhof, M. Generalized gradient approximation made simple. *Phys. Rev. Lett.* **77**, 3865–3868 (1996).

42. Tang, W., Sanville, E. & Henkelman, G. A grid-based Bader analysis algorithm without lattice bias. *J. Phys. Condens. Matter* **21**, 084204 (2009).
43. Sanville, E., Kenny, S. D., Smith, R. & Henkelman, G. Improved grid-based algorithm for Bader charge allocation. *J. Comput. Chem.* **28**, 899–908 (2007).
44. Wang, V., Xu, N., Liu, J. C., Tang, G. & Geng, W. T. Vaspkit: a user-friendly interface facilitating high-throughput computing and analysis using VASP code. *Comput. Phys. Commun.* **267**, 108033 (2021).
45. Henkelman, G., Arnaldsson, A. & Jónsson, H. A fast and robust algorithm for bader decomposition of charge density. *Comput. Mater. Sci.* **36**, 354–360 (2006).

Acknowledgements

This work was supported by the National Key R&D Program of China (2023YFA1507400), the National Natural Science Foundation of China (U24A20498, 22122901, 22402056), Changsha Natural Science Foundation (kq2402052), National Science and Technology Council (NSTC) 113-2112-M-213-018 and the support from the beamline staffs at beamlines TPS 32A (Tender X-ray absorption spectroscopy beamline) at the National Synchrotron Radiation Research Center (NSRRC). The authors would like to thank Shiyanjia Lab (https://www.shiyanjia.com) for the FTIR analysis.

Author contributions

W.C., S.W., and Y.Z. conceived and supervised the project. M.L. conducted experiments and analyzed data. Y.J. performed the DFT calculations. Y.H. and Y.L. conducted XAS measurements. L.X., S.L., Y.W., Z.X., and R.W. helped with the data analysis. M.L. wrote the manuscript and W.C. provided suggestions. All authors discussed the results and commented on the manuscript.

Competing interests

The authors declare no competing interests.

Additional information

Supplementary information The online version contains supplementary material available at https://doi.org/10.1038/s41467-025-58001-3.

Correspondence and requests for materials should be addressed to Wei Chen or Yuqin Zou.

Peer review information *Nature Communications* thanks Jian Zhang, Yao Zheng, and the other, anonymous, reviewer(s) for their contribution to the peer review of this work. A peer review file is available.